

Incommensurability-Induced Enhancement of Superconductivity in One Dimensional Systems

Ricardo Oliveira,¹ Miguel Gonçalves,² Pedro Ribeiro,^{2,3} Eduardo V. Castro,^{1,3} and Bruno Amorim⁴

¹*Centro de Física das Universidades do Minho e Porto, LaPMET,
Departamento de Física e Astronomia, Faculdade de Ciências,
Universidade do Porto, 4169-007 Porto, Portugal*

²*CeFEMA, LaPMET, Instituto Superior Técnico,
Universidade de Lisboa, Av. Rovisco Pais, 1049-001 Lisboa, Portugal*

³*Beijing Computational Science Research Center, Beijing 100193, China*

⁴*Centro de Física das Universidades do Minho e Porto, LaPMET,
University of Minho, Campus of Gualtar, 4710-057, Braga, Portugal*

We show that incommensurability can enhance superconductivity in one dimensional quasiperiodic systems with s-wave pairing. As a parent model, we use a generalized Aubry-André model that includes quasiperiodic modulations both in the potential and in the hoppings. In the absence of interactions, the model contains extended, critical and localized phases for incommensurate modulations. Our results reveal that in a substantial region inside the parent critical phase, there is a significant increase of the superconducting critical temperature compared to the extended phase and the uniform limit without quasiperiodic modulations. We also analyse the results for commensurate modulations with period close to the selected incommensurate one. We find that while in the commensurate case, the scaling of the critical temperature with interaction strength follows the exponentially small weak-coupling BCS prediction for a large enough system size, it scales algebraically in the incommensurate case within the critical and localized parent phases. These qualitatively distinct behaviors lead to a significant incommensurability-induced enhancement of the critical temperature in the weak and intermediate coupling regimes, accompanied by an increase in the superconducting order parameter at zero temperature.

I. INTRODUCTION

The quantum phases of quasiperiodic quantum matter have attracted a great deal of interest in recent years due to cold atom experiments on Bose glasses and many-body localization (MBL) on the one hand [1–7], and the remarkable phenomena observed in moire systems [8, 9], that are generically quasiperiodic, on the other.

Quasiperiodicity is responsible for a plethora of interesting physics, with the paradigmatic example being the dramatic change in the localization properties of the wave function with [10–18] and without [19–34] interactions. In one dimension, quasiperiodic patterns can change the nature of electronic wave functions from plane-wave-like extended into exponentially localized. At the delocalized-localized critical point, the wave functions are very exotic, exhibiting multifractal properties [35]. The Aubry-André-Harper (AAH) model [19] is a stalwart model where the non-trivial localization properties mentioned above can be observed and studied. The on-site potential's single-frequency quasiperiodic modulation results in a spectrum-wide quantum criticality (SWQC), such that all the single-particle eigenstates undergo a delocalized-localized transition at a finite value of the potential strength. This finite critical value is determined by the model's self-duality, resulting in a transition quite distinct from typical Anderson localization that occurs at any finite value of uncorrelated disorder [36–39]. Significant effort has been devoted to comprehending the physics of single-particle localization in

1D quasiperiodic systems described by the Aubry-André model and generalizations that contain mobility edges and/or critical phases, where the eigenstates are multifractal at non-fine-tuned extended regions of the phase diagram [29, 30, 33, 34, 40–45]. In the interacting case, however, the bulk of previous research has centered on highly excited states in the middle of the many-body spectrum, in the context of many-body localization [10–18]. The interplay between order and quasiperiodicity has also been explored [46–51], but the study of superconductivity in quasiperiodic systems is still in its infancy [52, 53].

In the case of moire systems, incommensurability effects are often neglected in theoretical studies of their quantum phases of matter. However, these effects can be of crucial importance, as recently experimentally observed in incommensurate twisted trilayer graphene [9]. For electronic densities sufficiently away from charge neutrality, a quasiperiodic-induced high density of weakly dispersive states, with observable transport signatures, was detected. Remarkably, superconducting phases were found to arise precisely in this regime and their nature is still unknown. This work opened the way for the study of quasiperiodic phenomena in moire materials experimentally, which in turn begs for a better theoretical understanding of the interplay between quasiperiodicity and interactions. Specifically, it is important to understand the nature of superconducting phases in the presence of strong quasiperiodic effects.

Motivated by the aforementioned theoretical gaps, in

this work we focus on the study of the interplay between superconductivity and quasiperiodicity in a generalization of the AAH model, that also includes an off-diagonal quasiperiodic modulation of the hoppings [26, 29]. The latter mimicks more closely the tunneling quasiperiodicity existing in moiré systems. Besides extended and localized phases, this model also includes a critical phase, where the wave function is delocalized in both real and momentum-space. Single-particle eigenstates with similar features were also theoretically predicted to arise in flatband regimes of moiré systems [54–56]. A natural question that arises is what types of superconducting states can emerge from the non-interacting multifractal parent state, once interactions come into play.

Recently, it was found that the 1D AAH model exhibits an enhancement of the critical temperature due to the multifractal structure of the non-interacting wave functions at the delocalization-localization transition. This suggests an intriguing relation between incommensurability and superconductivity [52], resembling the multifractality-induced increase of the critical temperature for disordered systems [57, 58]. Additionally, in systems with SWQC, a mean-field BdG approach has shown that the multifractality of single-particle wave functions can enhance matrix elements, leading to a pairing amplitude that is maximized near the metal-insulator transition, while still retaining phase coherence, therefore allowing for the existence of a superconductor dome near the critical point of the system [53].

In the present work, we employ a self-consistent Bogoliubov-de Gennes (BdG) approach [59, 60] to study s-wave superconductivity in the aforementioned generalized AAH model. We found a significant increase in the superconducting critical temperature in a substantial region of the critical phase, compared to the extended phase. By comparing the results for commensurate and incommensurate systems, we also found that even though in the former case the critical temperature has a BCS scaling with the interaction strength for a large enough system size, in the latter it scales algebraically, leading to a very significant enhancement of the critical temperature at small interaction strength.

We also discovered that while for commensurate systems, the critical temperature follows exponentially small weak-coupling BCS scaling with the interaction strength for sufficiently large system sizes, in incommensurate systems it scales algebraically both in the critical and localized parent phases. This qualitative difference leads to a substantial increase in the critical temperature in incommensurate systems at small interaction strengths, highlighting the significant impact of quasiperiodicity on the superconducting properties of the system.

II. MODEL AND METHODS

Model and BdG Hamiltonian

We will study superconductivity on the generalized 1D AAH model, which is described by the following Hamiltonian [26, 29]

$$\hat{H}_0 = \sum_{\sigma,m} [-t + V_2 \cos(2\pi Q[m+1])] c_{m+1,\sigma}^\dagger c_{m,\sigma} + \text{H.c.} - \sum_{\sigma,m} [V_1 \cos(2\pi Qm) + \mu] c_{m,\sigma}^\dagger c_{m,\sigma}. \quad (1)$$

where the first term contains uniform and modulated nearest-neighbor hoppings, while the second term contains a modulated potential. We consider a chain with N sites ($m \in \{0, 1, \dots, N-1\}$) and we adopt closed boundary conditions. As in the original AAH model, V_1 is the amplitude and $2\pi Q$ is frequency of the on-site potential. Additionally, this generalized model includes an off-diagonal modulation of the hopping parameters with amplitude V_2 and the same frequency $2\pi Q$. From this point on, we will take $t = 1$, i.e., all energies will be in units of t .

The model can also be seen as the reduction of a 2D Quantum Hall system with isotropic next-nearest-neighbor hoppings to a one-dimensional 1D chain. Its incommensurate nature emerges when either the on-site or the off-diagonal modulations are made quasiperiodic by choosing $Q \in \mathbb{R} \setminus \mathbb{Q}$, i.e., setting the frequency equal to an irrational number. In this work, we take $\frac{\sqrt{5}-1}{2}$ for our studies of the incommensurate case. Given that our aim is to construct a finite system with periodic boundary conditions, we can use rational approximants of Q by resorting to the Fibonacci numbers. In terms of Fibonacci rational approximants, Q can be written asymptotically as

$$Q = \lim_{n \rightarrow \infty} \frac{F_{n-1}}{F_n}, \quad (2)$$

where the Fibonacci sequence $\{F_n\}$ is defined recursively via the relation $F_n = F_{n-1} + F_{n-2}$ with $F_0 = F_1 = 1$. To compare incommensurate and commensurate systems, we built systems with similar sizes but with different choices of rational approximants. Specifically, if we fix the system size at $N = F_n$, we can examine systems with lower order rational approximants, $i < n$, where the modulation frequency is given by $Q_i = F_{i-1}/F_i$ and the system size is chosen to be $N_i = N_{\text{cell}} F_i \approx N$ for a fair comparison between the commensurate and incommensurate cases. Here, N_{cell} denotes the number of unit cells contained within the system of size N_i . By increasing the value of N_{cell} while keeping N fixed, we can approach the periodic/commensurate limit.

The localization phase diagram for the model in Eq. 1 in the plane (V_1, V_2) for the incommensurate system

was first studied by Han *et al.* [26]. For any energy, the eigenstates are extended for $\{V_1 < 2t \wedge V_2 < t\}$, localized for $\{V_1 > 2 \max(t, V_2)\}$, and critical for $\{V_2 > \frac{1}{2} \max(2t, V_1)\}$. Furthermore, the eigenstates are critical along the AAH transition line $\overline{AB} = \{V_1 = 2t \wedge V_2 < t\}$ and bicritical along the lines $\overline{BC} = \{V_2 = t \wedge V_1 < 2t\}$ and $\overline{BD} = \{V_2 = V_1/2 \wedge V_1 \geq t\}$.

In the calculations that follow, we adjust the chemical potential μ for each point (V_1, V_2) in the phase diagram in order to ensure that the free system is always at half-filling. This is particularly important for points in the diagram whose spectrum is not symmetric and other choices of chemical potential could result in the suppression of superconductivity simply due to gaps in the free spectrum.

To study the effects of the incommensurate nature of the generalized AAH model on superconductivity, we include a simple interaction term in our Hamiltonian. Specifically, the total Hamiltonian will include an attractive on-site Hubbard term

$$\hat{H} = \hat{H}_0 - g \sum_m c_{m\uparrow}^\dagger c_{m\downarrow}^\dagger c_{m\downarrow} c_{m\uparrow}, \quad (3)$$

which is defined by a single interaction parameter g . Within a mean-field approximation, we can define the on-site gap parameter as $\Delta_m \equiv -g \langle c_{m\downarrow} c_{m\uparrow} \rangle$ and write the Bogoliubov-de Gennes (BdG) Hamiltonian as

$$\hat{H}_{\text{BdG}} = \frac{1}{2} \Psi^\dagger \begin{pmatrix} \mathbf{h} & -\Delta & 0 & 0 \\ -\Delta^\dagger & -\mathbf{h}^* & 0 & 0 \\ 0 & 0 & \mathbf{h} & \Delta \\ 0 & 0 & \Delta^\dagger & -\mathbf{h}^* \end{pmatrix} \Psi, \quad (4)$$

where $\Psi \equiv \left(\mathbf{c}_\downarrow \ \mathbf{c}_\uparrow^\dagger \ \mathbf{c}_\uparrow \ \mathbf{c}_\downarrow^\dagger \right)^T$, such that the operators \mathbf{c}_σ and $\mathbf{c}_\sigma^\dagger$ are column vectors with N entries, for a lattice with N total sites, and we defined the matrices $(\mathbf{h})_{i,j} = H_{0;i,j}$ and $(\Delta)_{i,j} = \Delta_i \delta_{i,j}$. In this basis, it is evident that the BdG Hamiltonian is block-diagonalizable for a system without spin-orbit coupling or spin-flip terms. The BdG canonical transformation amounts to introducing a unitary transformation that diagonalizes the first block in H_{BdG} :

$$\begin{pmatrix} \mathbf{c}_\downarrow \\ \mathbf{c}_\uparrow^\dagger \end{pmatrix} = \begin{pmatrix} \mathbf{U} & -\mathbf{V}^* \\ \mathbf{V} & \mathbf{U}^* \end{pmatrix} \begin{pmatrix} \gamma \\ \gamma^\dagger \end{pmatrix}.$$

having the eigenvectors of H_{BdG} as columns and arranged such that all negative eigenvalues are in the $(\mathbf{U} \ \mathbf{V})^T$ columns and the positive eigenvalues are in the $(-\mathbf{V}^* \ \mathbf{U}^*)^T$ columns. The gap parameters are then determined self-consistently by using

$$\Delta_i = -g \sum_{\mu}^{\{E_\mu < 0\}} U_{i,\mu} V_{i,\mu}^* \tanh\left(\frac{E_\mu}{2k_B T}\right). \quad (5)$$

Our mean-field approach involves diagonalizing the BdG Hamiltonian (4) successively, while subject to the self-consistent equation (5), until convergence is attained. We use the relative error between two consecutive iterations of the mean-field parameters vector, which in this case is the gap parameters vector Δ_i , as our convergence criterion. The relative error is defined at the expense of the norm of these vectors as

$$\epsilon = \frac{\|\Delta^{M+1} - \Delta^M\|}{\|\Delta^{M+1}\|}, \quad (6)$$

for two consecutive iterations M and $M+1$. We chose to terminate our algorithm when $\epsilon < 10^{-4}$, which can take up to 50 iterations to reach convergence in the localized phase.

Although the BdG method is an excellent approach for analysing superconducting properties of one dimensional systems for temperatures below the superconducting critical temperature, it is not very efficient for computing the critical temperature itself. This is due to the large number of iterations required to obtain convergence near the temperature-driven transition. Instead, within the same mean-field approximation, a more appropriate method for this task is the linear gap equation. Following the approach in Ref. [52], the critical temperature can be computed from the linear gap equation in the Anderson approximation, valid in the weak-coupling limit, which can be written as

$$\Delta^\lambda = g \sum_{\lambda'} M_{\lambda,\lambda'} \frac{\tanh\left[\frac{E_{\lambda'}}{2k_B T}\right]}{2E_{\lambda'}} \Delta^{\lambda'}, \quad (7)$$

where $M_{\lambda,\lambda'} \equiv \sum_i |\phi_i^\lambda|^2 |\phi_i^{\lambda'}|^2$ is computed from the eigenstates ϕ_i^λ with eigenvalue E_λ of \hat{H}_0 . This is an eigenvalue problem for the gap parameters $\{\Delta^\lambda\}$ in the eigenbasis of \hat{H}_0 , and T_c can be computed from the greater eigenvalue of the gap equation matrix.

Inverse participation ratio analysis of localization properties

A useful quantity to study the localization properties of the eigenstates of a quasiperiodic system is the inverse participation ratio (IPR), which quantifies the fraction of the total probability density that is concentrated on a subset of lattice sites. For the free system, the IPR for a normalized eigenstate ϕ^λ corresponding to the E_λ eigenvalue can be defined as

$$\text{IPR}(E_\lambda) = \sum_{m=0}^N |\phi_m^\lambda|^4. \quad (8)$$

It is a well known result that for extended eigenstates, the IPR scales as N^{-1} in the thermodynamic limit ($n \rightarrow \infty$),

while for the localized states it tends to a finite value even in this limit. However, for critical multifractal states, the IPR scales as $N^{-\alpha}$ with $\alpha \in]0, 1[$ depending on the critical properties of the eigenstates.

A suitable quantity to study the localization phase diagram of the BdG Hamiltonian is the mean inverse participation ratio (MIPR) of the BdG wavefunctions,

$$\text{MIPR} = \frac{1}{2F_n} \sum_{\lambda=0}^{2F_n-1} \sum_{m=0}^{F_n-1} [U_{m,\lambda}^4 + V_{m,\lambda}^4]. \quad (9)$$

The slope of the MIPR varies rapidly near the transition lines between the extended, critical, or localized phases. Therefore, we can expect a jump in this quantity in the thermodynamic limit, which will allow us to compute the localization diagram for this system.

On the other hand, if we want to investigate the effects of localization on the gap parameters, we can define an IPR for the Δ_m , similar to what is done for the wave functions. The IPR for the Δ_m can be written as

$$\text{IPR}_{\Delta} = \frac{\sum_{m=0}^{F_n-1} |\Delta_m|^4}{\left[\sum_{m=0}^{F_n-1} |\Delta_m|^2 \right]^2}. \quad (10)$$

This is an energy-independent quantity, which characterizes the localization of Δ_m as a distribution on the lattice.

III. RESULTS

We applied the BdG method to the generalized AAH model with an on-site Hubbard term, at zero temperature, and for moderate values of the interaction parameter of the order of the uniform hopping parameter t . We found that it shares a similar localization diagram with the parent model, as shown in Fig.1(a). The MIPR exponent for the BdG wave functions allows us to define three phases, as in the free model: extended, critical, and localized. The exponent values are similar in the three regions and vary sharply close to the transition lines, juxtaposing on the critical lines of the free model. The mean-field algorithm converges smoothly for all points in the diagram, starting from a homogeneous initial proposal for the distribution of gap parameters.

However, unlike the free system that exhibits SWQC, we can see in Figs.1(b2) and 1(b4) along some representative lines in the (V_1, V_2) diagram that the BdG system exhibits some mobility edge structure. Although the transition occurs in the same way for most of the spectrum for the same critical value, we can see in Fig.1(b2) that the states close to the BdG gap transition from extended to localized for a critical value $V_1^c \gtrsim 2$. Additionally, in the transition from extended to critical, there is, again for the states close to the superconductor gap, a transition to critical states with a smaller IPR exponent α_n , that may

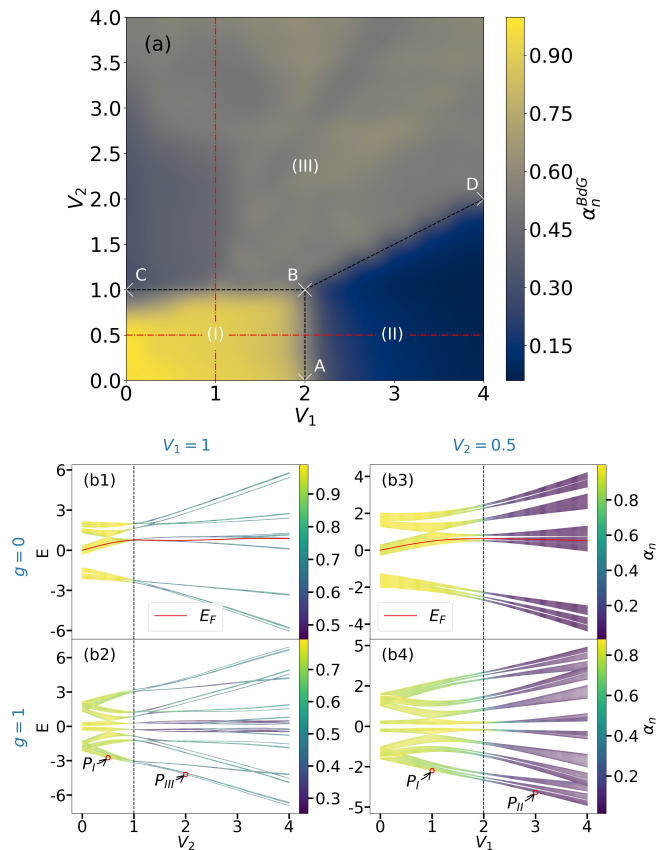


Figure 1. (a) $\alpha_n^{\text{BdG}} \equiv -\log[\text{MIPR}] / \log[F_n]$ for the BdG eigenstates in the (V_1, V_2) parameter space at zero temperature, with $g = 1$ for a system of size $N = F_n = 610$. α_n^{BdG} converges to 1 for extended states, 0 for localized states and to non-integer in-between values for critical states as $n \rightarrow \infty$. The transition lines \overline{AB} , \overline{BC} and \overline{BD} of the localization diagram for the free system are plotted as dashed black lines. The phases are (I) extended phase, (II) localized phase and (III) critical phase (b) Spectrum of \hat{H}_0 , for size $F_n = 2584$, and \hat{H}_{BdG} , for size $F_n = 610$, along representative (red-dashed) lines of the phase diagram in Fig.1(a). In the free system ($g = 0$), all eigenstates undergo the transition from extended to localized states at $V_1 = V_1^c = 2$ for $V_2 = 0.5$ (Fig.1(b3)), and from extended to critical states at $V_2 = V_2^c = 1$ for $V_1 = 1$ (Fig.1(b1)). However, this is only roughly true for the BdG system ($g = 1$), and we can see in Figs.1(b2) and 1(b4) that the spectrum exhibits some mobility edge structure. We represent, in color, $\alpha_n \equiv -\log[\text{IPR}] / \log[N]$.

even approach zero in the thermodynamic limit, which would indicate the presence of localized states.

We have concluded that the BdG wave functions in our model share a localization phase diagram that resembles that of the the generalized AAH model, apart from the appearance of mobility edges. We now aim to understand if the distribution of the gap parameters also has this behavior in the parameter space (V_1, V_2) . However, we found that although IPR_{Δ} is larger in the critical phase and even more so in the localized phase, the gap

parameters distribution never actually acquires a critical or localized structure. We can verify this by looking at some relevant points. Fig.2 shows the normalized Fourier transform of some BdG wave functions at the edge of the spectrum for some points of the diagram (V_1, V_2) , which are marked in Fig.1 as P_I , P_{II} , and P_{III} . We compare this BdG eigenstates structure with the gap parameters structure in momentum space for the same points in the diagram (V_1, V_2) . In phase I, the behavior is the same, with the BdG wave functions as well as the gap parameters having the same ballistic structure, evident in the exponentially localized peaks for some crystal momentum values. However, it is in the critical and localized phase that we see the greatest differences between these two scalar distributions. In phase III, the BdG functions suffer a partial delocalization around the ballistic peaks, acquiring a fractal distribution, corresponding to a critical distribution in real space. In phase III, they suffer a total delocalization in the first Brillouin zone, corresponding to a localization in real space. On the other hand, the distribution of gap parameters in momentum space is always ballistic for these two phases. The larger value of IPR_Δ is explained only by the appearance of more ballistic peaks for an extra small subset of momentum values.

To complete our analysis of the localization diagram for our model, we performed a finite-size analysis of both the MIPR of the BdG wave functions and the IPR_Δ for relevant points in the diagram (V_1, V_2) , in Fig.3. As mentioned in Sec.II, we should be able to perform a linear fit to $\text{IPR} \sim N^{-\alpha}$ in a log-log plot of IPR against the size of the system in the large N limit, allowing us to extrapolate and estimate the scaling exponent α . In Fig.3(a), we see that we enter this algebraic regime for a system of size $N = 610$, indicating that our localization diagram in Fig.1 is sufficiently converged to draw our previous conclusions. The algebraic scaling allows us to label phases I, II and III as extended, localized and critical, respectively. This confirms our result that the BdG wave functions are influenced by incommensurate modulations in the same way as the eigenstates of the free system.

It is noteworthy that in Fig.3(b), the $\text{IPR}_\Delta^I < \text{IPR}_\Delta^{II} < \text{IPR}_\Delta^{III}$ for all values of N . However, IPR_Δ scales with N in the same way as one would expect for a ballistic extended state. We can therefore rigorously conclude that the gap parameters do not share the localization properties of the BdG wave functions and the incommensurability of the underlying AAH system has little influence on the localization of the superconductor gap parameters.

In Fig.4(a), we report the critical temperature in the (V_1, V_2) parameter space of the generalized AAH model, computed using the linear gap equation (7). For a representative value of the interaction parameter, $g = 0.5$, the critical temperature is significantly higher in the localized phase II compared to the extended phase I. This

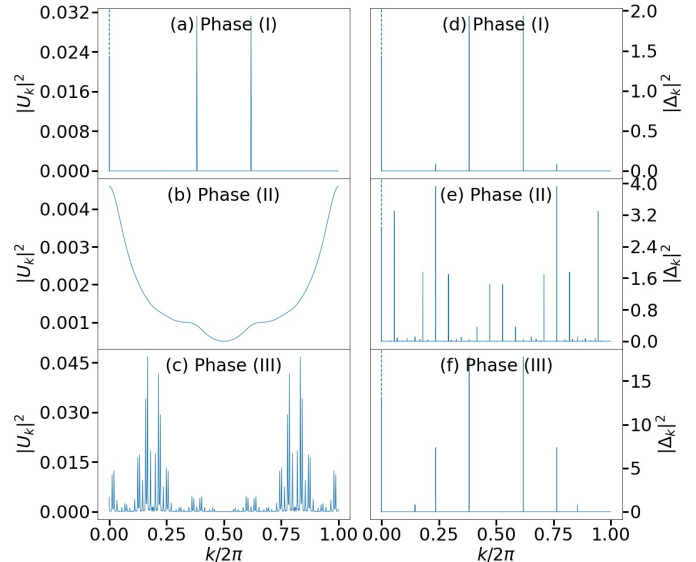


Figure 2. Momentum-space distribution of the BdG wave functions and of the gap parameters vector, for a system of size $N = F_n = 2584$ and interaction parameter $g = 1$. In (a)-(c) we plot the Fourier transform $|U_k|^2$ of the U -components of the BdG wave function at the lower edge of the spectrum ($E = E_{min}$). The chosen points are represented in Figs.1(b2) and (b4) as P_I , P_{II} , and P_{III} , corresponding to the points $(V_1, V_2) = (1, 0.5)$ (a), $(V_1, V_2) = (3, 0.5)$ (b) and $(V_1, V_2) = (1, 2)$ (c). Like its free system counterpart, in momentum-space it is ballistic in phase I (a), extended in phase II (b) and critical in phase III (c). The same cannot be said of the Fourier transform $|\Delta_k|^2$ of the gap parameters vector, represented in (d)-(f) for the same points in diagram (V_1, V_2) , which never exhibit a critical or extended structure like the momentum-space BdG wave functions, as we show more rigorously in Fig.3 with our finite-size analysis in real-space.

same enhancement also occurs in the critical phase III for small enough values of the on-site parameter, $V_1 \lesssim 1$. However, for larger values of V_1 in the critical phase, there is a suppression of the critical temperature. It is still higher than in the extended phase, but it attains smaller values if compared with the localized phase. In addition to this, we demonstrate, in Figs.4(c) and 4(d), the power-law behaviour of T_c with respect to g within the localized and critical phases of our generalized AAH model (with different exponents), in contrast to the BCS-like behaviour $T_c \sim \exp(-c/g)$ (where c depends on the non-interacting Hamiltonian parameters) in the extended phase (not shown). This is in good agreement to known results for the AAH model from Fan *et al.* [52]. We compare the incommensurate case with the commensurate to show that this power-law behavior is due to the incommensurate nature of our diagonal and off-diagonal

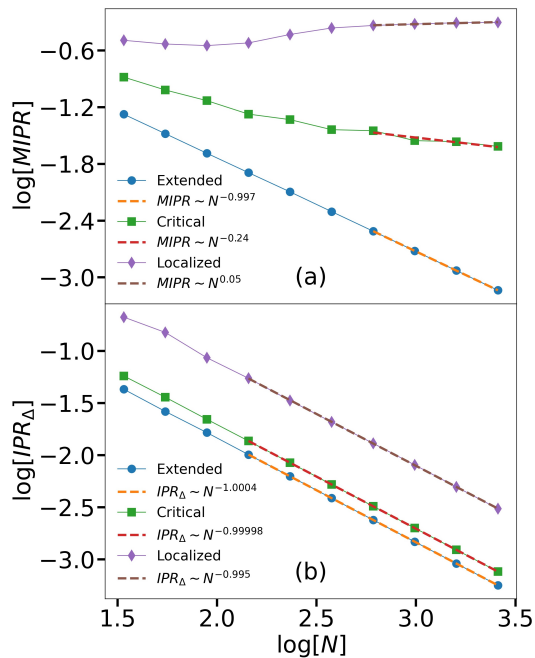


Figure 3. (a) Finite-size analysis of MIPR for the BdG wave functions, with $g = 1$. The log-log plot of MIPR as a function of the system size $N = F_n$ for 3 relevant points $(V_1, V_2) = (1, 0.5)$ (Extended phase I), $(V_1, V_2) = (3, 0.5)$ (Localized phase II) and $(V_1, V_2) = (1, 2)$ (Critical phase III). We perform a linear fit to $\text{IPR} \sim N^{-\alpha}$ for the larger system sizes, getting $\alpha_I^{\text{BdG}} = 0.997 \pm 0.001$, $\alpha_{II}^{\text{BdG}} = 0.05 \pm 0.02$ and $\alpha_{III}^{\text{BdG}} = 0.24 \pm 0.05$. (b) The same analysis is done for IPR_Δ . Even though $\text{IPR}_\Delta^I < \text{IPR}_\Delta^{II} < \text{IPR}_\Delta^{III}$, as expected, we found that this quantity has an extended-like scaling in all 3 phases.

quasiperiodic modulations. We observe in Figs.4(c) and 4(d), that in the incommensurate case ($N_{\text{cell}} = 1$) there is a power-law scaling of T_c with g . However, as we increase the number of unit cells up to $N_{\text{cell}} = 517$, we eventually obtain the BCS scaling expected for an homogeneous superconductor in BCS theory. The fact that we need to build a system with a large number of unit cells to achieve a BCS scaling implies that the incommensurate effects on the critical temperature resulting in the algebraic scaling are quite robust.

Moreover, we have obtained a similar (V_1, V_2) diagram at zero temperature using the BdG method for a different energy scale. From the gap parameters in the real-space basis, we can construct a scalar “order parameter” defined as $\max|\Delta|$, which provides a reasonable measure of the magnitude of the local superconductor pairing. In Fig.4(b), we show a distribution of this scalar in the space of modulation amplitudes (V_1, V_2) that is similar to the one found for the critical temperature in Fig.4(a). This is a surprising result because these different quantities are associated with different phenomena, one being the thermal energy at which the superconductor pairing vanishes, computed with the linear gap equation, and the other be-

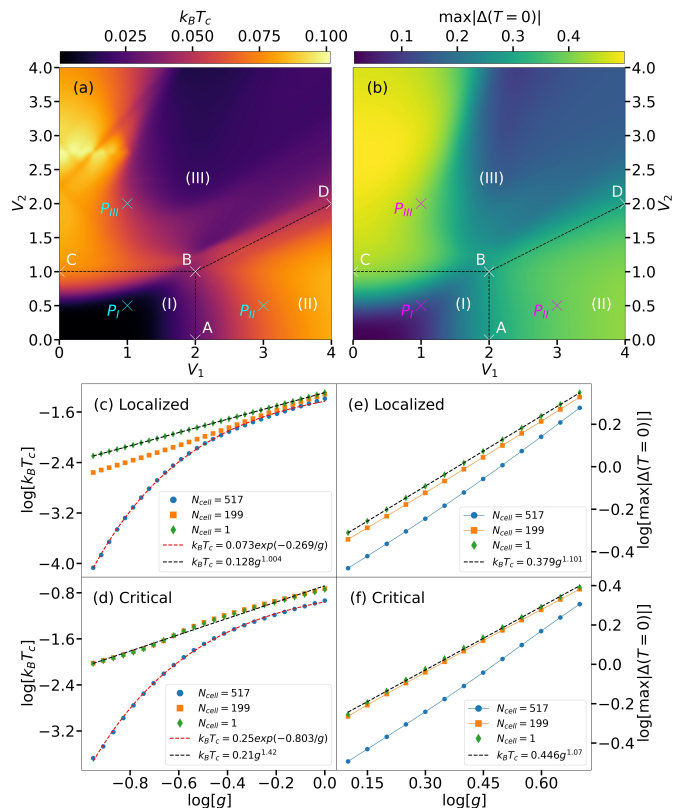


Figure 4. (a) (V_1, V_2) diagram of $k_B T_c$ computed with the linear gap equation (7), for $g = 0.5$ and $N = 987$. (b) (V_1, V_2) diagram of $\max|\Delta(T=0)|$ computed with the BdG method, for $g = 1$ and $N = 610$. (c)-(f) Scaling with g for different numbers of unit cells $N_{\text{cell}} \in \{1, 199, 517\}$, corresponding to $Q_i \in \{1597/2584, 8/13, 3/5\}$, respectively. The black-dashed lines correspond to the power-law fits, while the red-dashed ones correspond to the BCS fits. (c) and (d) are the $k_B T_c$ results for the localized and critical phases, respectively. (e) and (f) are the $\max|\Delta(T=0)|$ results for the localized and critical phases, respectively. The representative points of both these phases are marked as P_{II} and P_{III} in Figs.4(a) and 4(b).

ing the superconductor pairing amplitude at zero temperature, computed with the BdG method. This indicates that the underlying generalized AAH model strongly determines the behavior of these superconductivity properties. Additionally, similarly to the critical temperature, we found a power-law behavior $\max|\Delta| \sim g^\eta$ in the localized and critical phases. When we compare the commensurate case with the incommensurate case, we once again observe an algebraic enhanced scaling due to incommensurability, but we do not find a BCS scaling for the commensurate case.

IV. DISCUSSION

By studying a generalized AAH model with s-wave pairing, we were able to analyse the interplay between

superconductivity and quasiperiodicity in extended, localized and critical quantum phases. Within the critical phase, we found that the critical temperature acquires a power-law scaling with the interaction parameter g . We have demonstrated that this behaviour is a direct consequence of the incommensurate nature of the underlying model, by showing that in the commensurate case, the scaling reverts back to what is predicted by BCS theory for a uniform system. It was suggested in [52] that the opening of a superconductor gap in the quasiparticle spectrum could mask the localization transition at low temperatures for the original AAH model. However, by analyzing the localization of the BdG wavefunctions at zero temperature, we can conclude that not only is it possible to observe the localization transition of the original AAH, but that all single-particle localization transitions of the generalized AAH are preserved by the BdG Hamiltonian for s-wave pairing, despite the spectrum acquiring a slight mobility edge structure. We finally showed that the pairing amplitude calculated at zero temperature with BdG also scales algebraically with the interaction parameter, being enhanced in the incommensurate limit. Studying the behavior of superfluid stiffness in the (V_1, V_2) diagram at zero temperature could be interesting in the future. This could help us get a better understanding of how to fine-tune the modulations amplitudes in order to achieve superconductivity. Keeping in-line with the reasoning of [52, 53], the transition lines of the generalized AAH model could represent the perfect trade-off point between non-null superconducting pairing and phase coherence associated with a non-zero superfluid stiffness.

Our results show that incommensurability effects can be of crucial importance in shaping the nature of the superconducting state, particularly in parent phases where the localization properties differ from the uniform case. Higher dimensional systems also exhibit similar quasiperiodic-driven phases [32, 54, 55]. We therefore anticipate that in these systems, incommensurability effects will also play a critical role in understanding superconducting phases, in strong quasiperiodic regimes, such as those recently observed in [9] for twisted trilayer graphene. We leave the exploration of the interplay between superconductivity and quasiperiodicity in 2D for future work.

[1] G. Roati, C. D’Errico, L. Fallani, M. Fattori, C. Fort, M. Zaccanti, G. Modugno, M. Modugno, and M. Inguscio, *Nature* **453**, 895 (2008).
 [2] M. Schreiber, S. S. Hodgman, P. Bordia, H. P. Lüschen, M. H. Fischer, R. Vosk, E. Altman, U. Schneider, and I. Bloch, *Science* **349**, 842 (2015).
 [3] P. Bordia, H. P. Lüschen, S. S. Hodgman, M. Schreiber, I. Bloch, and U. Schneider, *Phys. Rev. Lett.* **116**, 140401

(2016).
 [4] P. Bordia, H. Lüschen, S. Scherg, S. Gopalakrishnan, M. Knap, U. Schneider, and I. Bloch, *Phys. Rev. X* **7**, 041047 (2017).
 [5] H. P. Lüschen, P. Bordia, S. Scherg, F. Alet, E. Altman, U. Schneider, and I. Bloch, *Phys. Rev. Lett.* **119**, 260401 (2017).
 [6] F. A. An, K. Padavić, E. J. Meier, S. Hegde, S. Ganeshan, J. H. Pixley, S. Vishveshwara, and B. Gadway, *Phys. Rev. Lett.* **126**, 040603 (2021).
 [7] T. Kohlert, S. Scherg, X. Li, H. P. Lüschen, S. Das Sarma, I. Bloch, and M. Aidelsburger, *Phys. Rev. Lett.* **122**, 170403 (2019).
 [8] L. Balents, C. R. Dean, D. K. Efetov, and A. F. Young, *Nat. Phys.* **16**, 725 (2020).
 [9] A. Uri, S. C. de la Barrera, M. T. Randeria, D. Rodan-Legrain, T. Devakul, P. J. D. Crowley, N. Paul, K. Watanabe, T. Taniguchi, R. Lifshitz, L. Fu, R. C. Ashoori, and P. Jarillo-Herrero, “Superconductivity and strong interactions in a tunable moiré quasiperiodic crystal,” (2023), [arXiv:2302.00686 \[cond-mat.mes-hall\]](https://arxiv.org/abs/2302.00686).
 [10] S. Iyer, V. Oganesyan, G. Refael, and D. A. Huse, *Phys. Rev. B* **87**, 134202 (2013).
 [11] V. Khemani, D. N. Sheng, and D. A. Huse, *Phys. Rev. Lett.* **119**, 075702 (2017).
 [12] M. Lee, T. R. Look, S. P. Lim, and D. N. Sheng, *Phys. Rev. B* **96**, 075146 (2017).
 [13] R. Mondaini and M. Rigol, *Phys. Rev. A* **92**, 041601 (2015).
 [14] R. Modak and S. Mukerjee, *Phys. Rev. Lett.* **115**, 230401 (2015).
 [15] M. Žnidarič and M. Ljubotina, *Proceedings of the National Academy of Sciences* **115**, 4595 (2018), <https://www.pnas.org/doi/pdf/10.1073/pnas.1800589115>.
 [16] S. Xu, X. Li, Y.-T. Hsu, B. Swingle, and S. Das Sarma, *Phys. Rev. Res.* **1**, 032039 (2019).
 [17] E. V. H. Doggen and A. D. Mirlin, *Phys. Rev. B* **100**, 104203 (2019).
 [18] D. Vu, K. Huang, X. Li, and S. Das Sarma, *Phys. Rev. Lett.* **128**, 146601 (2022).
 [19] S. Aubry and G. André, *Ann. Israel Phys. Soc* **3**, 18 (1980).
 [20] J. B. Sokoloff, *Phys. Rev. B* **22**, 5823 (1980).
 [21] M. Kohmoto, L. P. Kadanoff, and C. Tang, *Phys. Rev. Lett.* **50**, 1870 (1983).
 [22] D. J. Thouless, *Phys. Rev. B* **28**, 4272 (1983).
 [23] M. Kohmoto and J. R. Banavar, *Phys. Rev. B* **34**, 563 (1986).
 [24] C. Tang and M. Kohmoto, *Phys. Rev. B* **34**, 2041 (1986).
 [25] Y. G. Sinai, *Journal of Statistical Physics* **46**, 861 (1987).
 [26] J. H. Han, D. J. Thouless, H. Hiramoto, and M. Kohmoto, *Phys. Rev. B* **50**, 11365 (1994).
 [27] I. Chang, K. Ikezawa, and M. Kohmoto, *Phys. Rev. B* **55**, 12971 (1997).
 [28] Y. Takada, K. Ino, and M. Yamanaka, *Phys. Rev. E* **70**, 066203 (2004).
 [29] F. Liu, S. Ghosh, and Y. Chong, *Physical Review B* **91** (2014), [10.1103/PhysRevB.91.014108](https://doi.org/10.1103/PhysRevB.91.014108).
 [30] J. Wang, X.-J. Liu, G. Xianlong, and H. Hu, *Phys. Rev. B* **93**, 104504 (2016).
 [31] Q.-B. Zeng, S. Chen, and R. Lü, *Phys. Rev. B* **94**, 125408 (2016).
 [32] T. Devakul and D. A. Huse, *Phys. Rev. B* **96**, 214201 (2017).

- [33] T. Liu, P. Wang, S. Chen, and G. Xianlong, *Journal of Physics B: Atomic, Molecular and Optical Physics* **51**, 025301 (2017).
- [34] M. Yahyavi, B. Hetényi, and B. Tanatar, *Phys. Rev. B* **100**, 064202 (2019).
- [35] F. Evers and A. Mirlin, *Rev. Mod. Phys.* **80**, 1355 (2008).
- [36] E. Abrahams, P. W. Anderson, D. C. Licciardello, and T. V. Ramakrishnan, *Physical Review Letters* **42**, 673 (1979), [arXiv:1208.1722](#).
- [37] D. Vollhardt and P. Wölfle, *Phys. Rev. B* **22**, 4666 (1980).
- [38] A. MacKinnon and B. Kramer, *Phys. Rev. Lett.* **47**, 1546 (1981).
- [39] B. Kramer and A. MacKinnon, *Rep. Prog. Phys.* **56**, 1469 (1993).
- [40] J. Biddle and S. Das Sarma, *Phys. Rev. Lett.* **104**, 70601 (2010).
- [41] J. D. Bodyfelt, D. Leykam, C. Danieli, X. Yu, and S. Flach, *Phys. Rev. Lett.* **113**, 236403 (2014).
- [42] S. Ganeshan, J. H. Pixley, and S. Das Sarma, *Phys. Rev. Lett.* **114**, 146601 (2015).
- [43] X. Deng, S. Ray, S. Sinha, G. V. Shlyapnikov, and L. Santos, *Phys. Rev. Lett.* **123**, 025301 (2019).
- [44] Y. Wang, L. Zhang, S. Niu, D. Yu, and X.-J. Liu, *Phys. Rev. Lett.* **125**, 073204 (2020).
- [45] T. Liu, X. Xia, S. Longhi, and L. Sanchez-Palencia, *SciPost Phys.* **12**, 27 (2022).
- [46] J. Vidal, D. Mouhanna, and T. Giamarchi, *Phys. Rev. Lett.* **83**, 3908 (1999).
- [47] C. Schuster, R. A. Römer, and M. Schreiber, *Phys. Rev. B* **65**, 115114 (2002).
- [48] P. Naldesi, E. Ercolessi, and T. Roscilde, *SciPost Phys.* **1**, 010 (2016).
- [49] D. Vu and S. Das Sarma, *Phys. Rev. Lett.* **126**, 036803 (2021).
- [50] A. Chandran and C. R. Laumann, *Phys. Rev. X* **7**, 031061 (2017).
- [51] P. J. D. Crowley, C. R. Laumann, and A. Chandran, *Journal of Statistical Mechanics: Theory and Experiment* **2022**, 083102 (2022).
- [52] Z. Fan, G.-W. Chern, and S.-Z. Lin, *Phys. Rev. Res.* **3**, 023195 (2021).
- [53] X. Zhang and M. S. Foster, *Phys. Rev. B* **106**, L180503 (2022).
- [54] Y. Fu, E. J. König, J. H. Wilson, Y.-Z. Chou, and J. H. Pixley, *npj Quantum Materials* **5**, 71 (2020).
- [55] M. Gonçalves, H. Z. Olyaei, B. Amorim, R. Mondaini, P. Ribeiro, and E. V. Castro, *2D Materials* **9**, 011001 (2021).
- [56] Y.-Z. Chou, Y. Fu, J. H. Wilson, E. J. König, and J. H. Pixley, *Phys. Rev. B* **101**, 235121 (2020).
- [57] M. V. Feigel'man, L. B. Ioffe, V. E. Kravtsov, and E. A. Yuzbashyan, *Phys. Rev. Lett.* **98**, 027001 (2007).
- [58] K. Zhao, H. Lin, X. Xiao, W. Huang, W. Yao, M. Yan, Y. Xing, Q. Zhang, Z.-X. Li, S. Hoshino, J. Wang, S. Zhou, L. Gu, M. S. Bahramy, H. Yao, N. Nagaosa, Q.-K. Xue, K. T. Law, X. Chen, and S.-H. Ji, *Nature Physics* **15**, 904 (2019).
- [59] P. De Gennes and P. Pincus, *Superconductivity Of Metals And Alloys*, Advanced Books Classics (Avalon Publishing, 1999).
- [60] D. J. Scalapino, S. R. White, and S. Zhang, *Phys. Rev. B* **47**, 7995 (1993).